Acta Mech
DOI 10.1007/s00707-013-0922-2

E. J. Tozzi · D. M. Lavenson · M. J. McCarthy · R. L. Powell

Effect of fiber length, flow rate, and concentration on velocity profiles of cellulosic fiber suspensions

Received: 21 November 2012 / Revised: 26 March 2013

Abstract Conversion of cellulosic biomass to useful products involves pumping and mixing of fiber suspensions. Depending upon the concentration, the fibers may entangle to form flocs and networks. The fibers in these suspensions may settle both as individual fibers and fiber flocs. The flow of cellulosic suspensions has been previously modeled using generalized Newtonian rheological models. Under some flow conditions, those models do not apply due to strong gravitational effects that result in concentration gradients. Magnetic resonance flow imaging was used to obtain velocity profiles of fiber suspensions in horizontal pipe flow as a function of fiber length, concentration, and flow rates. Measures of flatness and asymmetry are used to characterize the shape of the velocity profiles. The largest asymmetry is found near a crowding number of roughly three. At higher crowding numbers, the velocity profiles tended to become flat, more symmetric, and pressure drops per unit length depend strongly on concentration.

1 Introduction

Cellulosic suspensions are prevalent in pulp and paper processing, paper making, food processing, and the rapidly developing area of conversion of biomass into fuels and chemicals. Design and optimization of these processes demand a comprehensive rheological characterization of the suspensions, which is challenging due to the interactions between fibers that form complex microstructures [1]. At sufficiently high concentrations, fibers can form mechanically connected networks that result in the suspensions having an apparent yield stress. These can be modeled as generalized Newtonian fluids with a yield stress [2–5]. Conventional rheometer measurements present numerous challenges due to the large size of fibers in relation to rheometer gaps and the heterogeneity of the suspensions that typically result in measurements with large uncertainties. Some factors that complicate the flow of fiber suspensions include the formation and disruption of flocs, fiber settling, the presence of air bubbles, and the formation of fiber-depleted layers in the vicinity of the boundaries of pipes or rheometers [1,6,7].

During the initial stages of hydrolysis, biomass fibers undergo rapid changes in shape [8], therefore understanding the influence of fiber length and diameter, specifically the aspect ratio (length/diameter), on rheology is necessary for both process design and control. In previous work, we showed that using magnetic resonance imaging to measure the yield stress of concentrated fiber suspensions flowing through a horizontal pipe overcomes the limitations of conventional rheometers. This noninvasive technique characterizes samples over a large suspension volume [9]. Pipes used for these studies have diameters that are much larger than either the fiber or floc sizes. Hence, the dimensions of the measuring geometry are much more similar to those in a typical processing plant than those in a conventional rheometer.

E. J. Tozzi · D. M. Lavenson · M. J. McCarthy · R. L. Powell (✉)
University of California, Davis, Davis, CA, USA
E-mail: rlpowell@ucdavis.edu

Published online: 17 September 2013

Table 1 Characteristics of fibers used

Variable	Fiber type		
	Short (200 EZ)	Medium (C100)	Long (pulp)
Mean length (LW, mm)	0.207	0.349	1.110
Mean length (NW, mm)	0.183	0.273	0.675
Mean width (LW, μm)	26.4	31.7	22.5
Number of profiles	77	102	70
Min. concentration (%w/w)	0.049	0.051	0.012
Max. concentration (%w/w)	18.4	11.4	1.88

The use of a generalized Newtonian model is valid as long as a suspension is homogeneous. At certain ranges of concentrations and flow rates that are sufficiently low, however, settling can occur, resulting in an effective medium with spatially varying properties. Vertically asymmetric velocity distributions due to buoyancy effects have been reported by Altobelli et al. [10], who measured velocity and concentration profiles of suspensions of spheres flowing in a horizontal pipe using magnetic resonance imaging. The flow of suspensions of settling particles has been modeled by Ramachandran and Leighton [11]. Their model describes viscous resuspension and upward secondary flows in the center of circular pipes.

In this work, we use magnetic resonance imaging to measure velocity profiles of fiber suspensions flowing through a horizontal pipe over a wide range of concentrations and flow rates, including those for which gravity causes asymmetry in the velocity profiles. Velocity profiles were strongly influenced by fiber length, fiber concentrations, and flow rates. Various features were observed including immobile layers at the bottom of the pipe, mobile networks that translate as a plug, and also asymmetric profiles that suggest concentration gradients along the vertical direction. To characterize the many types of complex velocity profiles observed, we propose to use measures of asymmetry and flatness. We map these measures in the concentration–flow rate plane to determine regions where settling causes the largest disturbances in velocity profiles. Knowing the location of such regions can be useful to decide whether or not to use generalized Newtonian rheological models. We will show that concentration effects are best described by the use of a crowding number [12] $N = 2/3\ \Phi\ a_r^2$, where Φ is the volume fraction and a_r is the aspect ratio, which is the length L divided by diameter D. Small crowding numbers correspond to concentration regimes in which fibers do not interact. As the crowding number increases, large changes in pressure and velocity profiles may occur over a narrow range of N. In the range of $N = 3$, it is generally considered [12] that a fiber network forms and the properties are dominated by strong interactions among fibers. The quadratic dependence on a_r clearly demonstrates that long fibers will have strong fiber–fiber interactions.

2 Materials and methods

Three types of fibers with different average particle aspect ratios were used. Short- and medium-length fibers were two grades (100 and 200 EZ), of commercial delignified cellulosic particles (Solka-Floc, International Fiber corporation, Tonawanda, NY). Long fibers were obtained from sheets of delignified pulp. Fiber sizes, shown in Table 1, were measured with a fiber analyzer. The length-weighted average length is defined as [13]

$$L_{LW} = \frac{\sum (l_i n_i)\, l_i}{\sum l_i n_i}, \tag{1}$$

where n_i is the number of fibers belonging to the length class l_i. The length-weighted average width is calculated using a similar approach, where fiber widths are averaged using fiber lengths as the weighting factors. The moisture content was measured using a Mettler Toledo model HR83 moisture analyzer (Mettler Toledo, Inc., Columbus, OH).

The pulp sheets were cut into sections 0.4 cm by 3 cm, weighed, mechanically dispersed in a measured amount of water using a mixer, and equilibrated at room temperature 24 h prior to the experiment.

Figure 1a is a schematic of the flow system used for these studies. The suspensions were loaded into a mixing tank (#1, Fig. 1a) connected to a Moyno positive displacement pump (#2, Fig. 1a, Moyno Inc., Springfield, OH) that pumps the suspension through an acrylic tube 2.08 m long with an internal diameter of 18.5 mm. The suspension flows through the imaging section of the magnetic resonance imaging (MRI) system (#3, Fig. 1a) and returns to the tank. Pressure drops (#4, Fig. 1a) and temperatures were measured at the ends

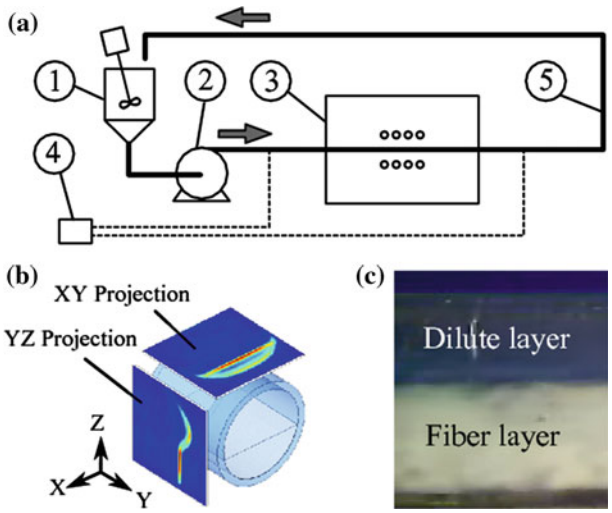

Fig. 1 **a** Flow imaging system used in the experiments: *1* agitated tank; *2* pump; *3* imaging magnet enclosure; *4* differential pressure transducer; *5* return line. **b** The magnetic resonance flow image projected in the YZ plane reveals asymmetry in a stratified flow. **c** Optical image of fiber suspension flowing along a horizontal pipe. An opaque layer of fibers moves in the lower region and a clear fluid layer at the *top* section

of the acrylic tube. Velocity profiles were obtained using a velocity-encoded pulsed gradient spin echo (PGSE) sequence on an Aspect Imaging MR2 1 T MRI spectrometer (Aspect Imaging, Shoham, Israel), with 30 G/cm peak gradient strength. The radio frequency coil for flow imaging is a solenoid with three turns, encasing a cylindrical volume 38 mm in diameter and 36 mm long. The velocity profiles obtained are projections of the 3D velocity profile onto a 2D plane (Fig. 1b). The 2D plane is vertical, so asymmetry in velocity profiles due to gravitational effects can be observed. More details on the technique can be found in Lavenson et al. [9].

Concentrations of fibers are presented as percent mass fraction

$$\%\mathrm{w/w} = X_\mathrm{m} \times 100 = \frac{m_\mathrm{f}}{m_\mathrm{f} + m_\mathrm{w}} \times 100, \tag{2}$$

where X_m is the mass fraction, m_f is the mass of fibers (dry basis), and m_w is the total mass of water including the water present as moisture in the fibers.

The volume fraction Φ is calculated from the mass fraction using [14]

$$\Phi = \frac{X_\mathrm{m}}{X_\mathrm{m} + \frac{\rho_\mathrm{f}}{\rho_\mathrm{w}}(1 - X_\mathrm{m})}, \tag{3}$$

where $\rho_\mathrm{f} = 1{,}500\,\mathrm{kg/m^3}$ is the density of the cellulose fibers, and $\rho_\mathrm{w} = 1{,}000\,\mathrm{kg/m^3}$ is the density of water. Since crowding numbers incorporate the fiber aspect ratio squared, two fiber types with the same mass concentration but different aspect ratio will have very different crowding numbers. For example, for $N = 1$, the concentration of the highest aspect ratio fibers used here needs to be only 0.092 % w/w, whereas for the lowest aspect ratio fibers, the concentration needs to be 3.61 % w/w.

The velocity profiles obtained are recorded as a set of points representing the MRI signal intensity as a function of y and z. The fluid flows in the positive y direction, and the y coordinate of a point is the maximum velocity of the fluid contained in an x–y slice located at a given vertical position z. The origin of the z axis is chosen as the center of the tube. For radially symmetric velocity profiles, the velocity is the same at vertical positions $+z$ and $-z$. The asymmetry, α, of a velocity profile is calculated from the difference between velocities in the top half of the profile $v(z)$ and the velocities at the same vertical position on the bottom half of the profile $v(-z)$, Fig. 2, using

$$\alpha = \sum_i \frac{|v(z_i) - v(-z_i)|}{\frac{1}{2}|v(z_i) + v(-z_i)|}, \tag{4}$$

where i represents the velocity data for a particular pixel and the summation is from 1 to n with n being the number of velocity points that constitute the half profile. The center of the pipe is located at vertical position

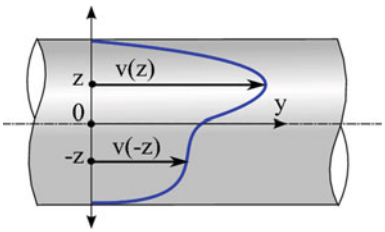

Fig. 2 To calculate the asymmetry factor α of velocity profiles, the velocity at a vertical position z is compared to the velocity at position $-z$. The difference is normalized with the average of both velocities

$z = 0$. The denominator $1/2|v(z_i) + v(-z_i)|$ is the average of the velocities on each half of the profile, and is used to make the asymmetry measure dimensionless and independent of the absolute velocities. For highly symmetric velocity profiles, $v(z)$ differs little from $v(-z)$ and low values of α are obtained. The range of values measured in this study was $5 \times 10^{-4} \leq \alpha \leq 2$.

The flatness measure of velocity profiles is calculated as $v_{\max} \langle v \rangle$, where the maximum velocity $v_{\max}$ is obtained from MRI images. For pipe flow, this means that in laminar flow, a Newtonian fluid has a flatness value of two and for plug flow, the flatness is one. Here, the average velocity is $\langle v \rangle = Q/A$, where Q is the volumetric flow rate and A the cross-section of the pipe. The volumetric flow rate was measured using timed collections of the suspension. Reynolds numbers used throughout this article are based on the density and viscosity of water for reference purposes. The viscosity and density of the suspensions are in general different from those of water, and these Reynolds numbers become less descriptive of the physics as the concentration of fibers is increased.

To characterize velocity in dimensionless form, we employ the buoyancy number [15], defined as

$$\mathrm{Bu} = \frac{(\rho_\mathrm{S} - \rho_\mathrm{L}) D^2 g}{18\, \mu \langle v \rangle},$$

where the densities ρ_S and ρ_L are the densities of the solid and liquid phases, D is the fiber diameter, g the acceleration of gravity, μ the viscosity of water, and $\langle v \rangle$ the bulk velocity.

An experiment was started by loading water into the flow system and adding a measured mass of fibers corresponding to the lowest concentration. Images were taken at various flow rates at this concentration. The flow rates were changed using a digital variable frequency drive. Timed collections were performed to record volumetric flow rates. To increase fiber concentration, measured amounts of fibers were added to the flow system and images were again taken at various flow rates.

A total of 249 velocity profiles were measured. The findings of the hundreds of profiles measured were catalogued by storing the experimental data for each fiber type into three arrays. The first array contained the logarithms of the crowding numbers. The second array contained the logarithms of the buoyancy number. The third array contained the asymmetry factor alpha for the first set of maps. For a second compilation of data, the third array contained the flatness measure. The arrays were processed using MATLAB, Release 2011a (The MathWorks, Inc., Natick, MA, USA). The function "TriScatteredInterp" was used to perform a linear interpolation and produce contour plots using a grid with a resolution of 0.1 units in each direction on logarithmic scales. The contour plots were post-processed using the vector graphics editor Inkscape, Release 0.48 (inkscape.org) to enhance legibility.

3 Results

Seven representative velocity profiles are shown in Fig. 3. The corresponding experimental conditions are listed in Table 2. The pressure drops, ΔP, are reported as $\Delta P / \Delta P_\mathrm{w}$, where ΔP_w is the pressure drop of water at the same flow rate. Water pressure drops are calculated using the Poiseuille formula for $Re < 2{,}100$. For $Re > 2{,}100$, we use the Serghides equation [16] with a tube relative roughness $\varepsilon/D = 1 \times 10^{-6}$. A comparison between these formulas and measured pressure drops of water is plotted in Fig. 4.

The first profile corresponds to water without fibers. The measure of asymmetry is $\alpha = 0.016$ (a perfectly symmetric profile would have $\alpha = 0$), whereas the ratio $v_{\max}/\langle v \rangle = 1.97$ is close to the theoretical value of 2 for a parabolic profile. These differences provide a measure of the accuracy of the measuring system.

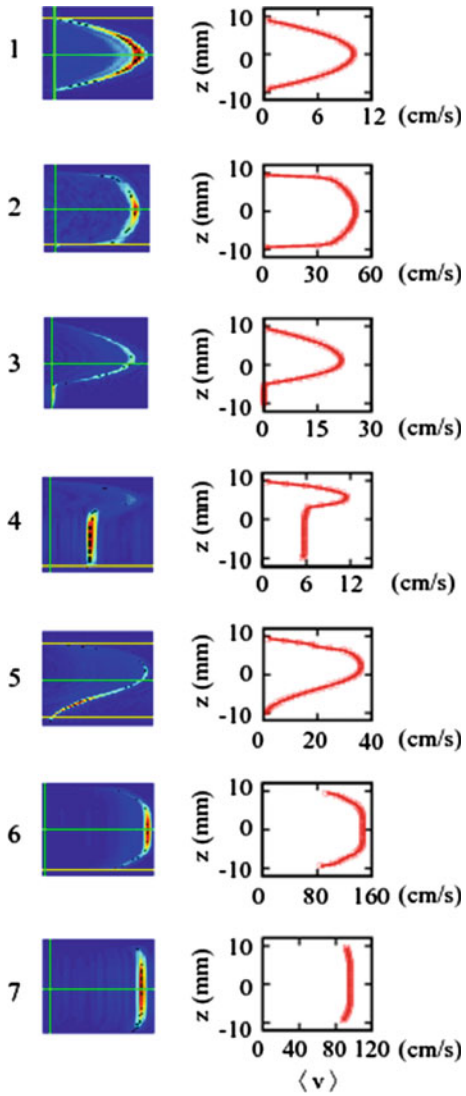

Fig. 3 Examples of various types of velocity profiles measured. The *left column* illustrates the MR images obtained, with added *lines* to indicate the zero velocity line, the center of the pipe and the *upper* and *lower* walls. The *right column* shows velocity profiles computed from the images. Experimental parameters corresponding to each profile are listed in Table 2

Table 2 Parameters of 7 profile examples illustrated in Fig. 3

Example	Suspension	α	$v_{\max}/\langle v\rangle$	$\Delta P/\Delta P_{\mathrm{w}}$	Re	$\langle v\rangle >$ (m/s)	N	C (%w/w)
1	Water	0.016	1.97	1.10	991	0.054	0.0	0.0
2	Short fibers	0.005	1.23	0.84	7,684	0.509	0.027	0.10
3	Short fibers	1.158	2.34	2.49	1,934	0.099	0.41	1.50
4	Long fibers	0.375	1.85	4.74	1,149	0.062	2.74	0.25
5	Medium fibers	0.713	1.92	1.67	3,726	0.201	1.71	3.14
6	Medium fibers	0.019	1.07	4.92	24,936	1.348	4.23	4.23
7	Medium fibers	0.005	1.01	42.3	17,307	0.935	6.41	11.44

At low flow rates, temperature differences may also influence measured velocity profiles and create asymmetry. Profile number 2 was obtained using a suspension with low concentration of low aspect ratio (short) fibers and a higher flow rate that for Profile 1. The velocity profile has a blunted shape with $v_{\max}/\langle v\rangle < 2$ characteristic of turbulent flows. The measure α is close to zero indicating a high degree of symmetry.

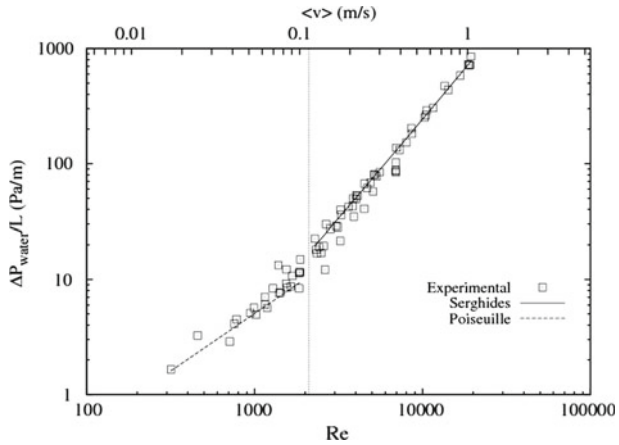

Fig. 4 Pressure drop per unit length $\Delta P/L$ (Pa/m) for water as a function of Reynolds number and average velocity. *Symbols* indicate experimental values, *lines* are plotted using the Poiseuille ($Re < 2{,}100$) and Serghides equations ($Re > 2{,}100$) for pressure drop in *cylindrical pipes*

Profile 3 has a well-defined settled layer of fibers at the bottom of the pipe that could be visually observed. The layer is immobile causing a large asymmetry in the profile. For Profile 4, obtained using high aspect ratio fibers with $N = 2.7$, there is also a well-defined settled layer, but this layer is mobile. High asymmetry and low flatness are also observed in this type of profile. The fifth profile shows asymmetry but the profile lacks the abrupt changes in velocity found in Profiles 3 and 4. The asymmetry of this type of profile is best interpreted in light of the experiments of Altobelli at al. [10] or the models of Ramachandran and Leighton [11], which show that particle concentrations may attain an asymmetric yet continuous distribution due to secondary flows. The continuous variation of suspension properties with position is reflected in the velocity profile. These types of profiles are observed at flow rates high enough to keep all particles in suspension but low enough that gravitational effects are noticeable. Profiles 6 and 7 are characterized by low α and high flatness. Such flat profiles were observed at the highest fiber concentrations. In Profile 6, a distinct central core is observed moving at constant velocity. The radius of such a plug has been used to calculate the yield stress of fiber suspensions [9]. Other profile shapes observed are ones that have a central core and some asymmetry, with an intermediate shape between Profiles 5 and 6.

3.1 Detecting asymmetric flows

In Fig. 5, we present contour maps of asymmetry as a function of concentration and flow rate. The coordinates in the plane are the crowding number N and the buoyancy number Bu, in a logarithmic scale. Concentrations increase from left to right in the figure. The flow rate increases from top to bottom, namely the points at the top of the graph have high buoyancy number (low average velocities) and the points at the bottom of the graph have low buoyancy number (high average velocities). The contours show the range of asymmetry measure α. Values of $\alpha > 0.05$ are considered asymmetric. Concentration is represented through $\log_{10} N$. The corresponding mass fraction of fibers can be found using Eq. (2). The average velocity, $\langle v \rangle = Q/A$, is used in the buoyancy number to represent the overall flow conditions. The corresponding Reynolds number Re based on water properties for a given value of $\langle v \rangle$ can be found in Fig. 4. The dotted line represents the extent of the experimental data.

In Fig. 5, it is observed that asymmetric profiles occur in regions of lower flow rates and at fiber concentrations below a certain limit. This limit is different for each fiber type in terms of mass fraction, but very similar in terms of crowding number. Highly symmetric profiles at low fiber concentrations occur during the transition to turbulence as the flow rates are increased. At high concentrations (i.e., $N > 3$), symmetric profiles are observed at all flow rates. The highest asymmetries are observed at concentrations near $N = 3$ and slightly lower. For concentrations that are much lower, the volume fraction of fibers is too small to noticeably influence the velocity profile. The results show the existence of regions where asymmetric profiles are prevalent. In these regions, models that account for buoyancy and secondary flows may be more appropriate [11] than models that assume homogeneous properties.

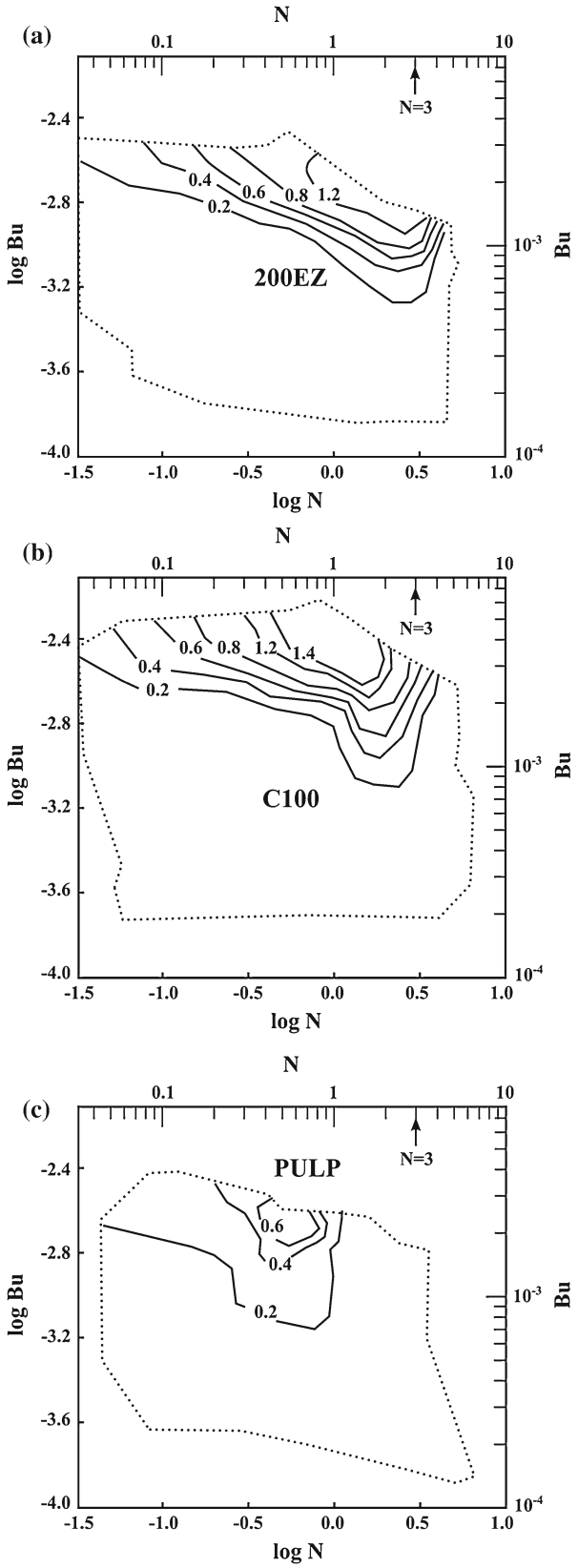

Fig. 5 Contours of the asymmetry measure α, as a function of the logarithm of the crowding number, N, and the logarithm of the Buoyancy number for 200 EZ, C 100 and pulp fibers. The *dotted line* indicates the scope of the experimental data

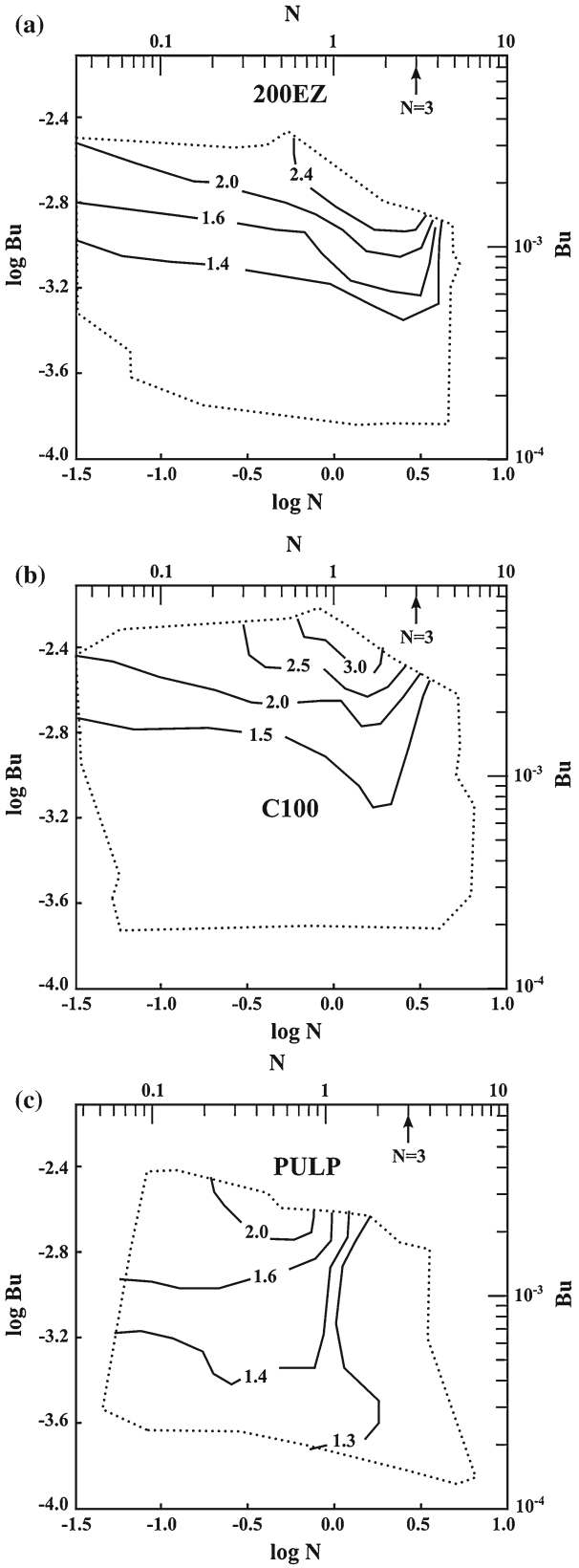

Fig. 6 Contours of the flatness measure, $v_{\max}/\langle v\rangle$, as a function of the logarithm of the crowding number, N, and the logarithm of the buoyancy number for 200 EZ, C100, and pulp fibers. The *dotted line* indicates the scope of the experimental data

Figure 6 shows the flatness measure $v_{max}/\langle v\rangle$. In laminar, symmetric flows of shear-thinning fluids, the flatness is between $1 \leq v_{max}/\langle v\rangle \leq 2$, where 1 corresponds to plug flow and 2 to a Newtonian fluid. Values of $v_{max}/\langle v\rangle > 2.1$ indicate strong settling. Profiles having flatness measures >2 tend to occur under the same conditions for which high asymmetry occurs, namely lower flow rates and at fiber concentrations slightly below crowding number $N = 3$. At high concentrations ($N > 3$), flat profiles are observed at all flow rates due to the formation of large plug-flow regions. Measurements of the pressure drop also show the influence of crowding number, with large increases in pressure drop being observed when $N \geq 3$.

The low asymmetries measured at large crowding numbers are expected in terms of formation of networks that are resistant to deformation. High particle concentrations are also known to hinder settling, therefore diminishing the influence of gravity. The strong asymmetries observed at intermediate and low concentrations, and low flow rates, however, reveal more intriguing aspects of fiber interactions. One of these is the existence of a concentration regime in which settling is not only hindered but "accelerated" due to fiber interactions. Herzhaft and Guazelli [17] measured sedimentation of fibers in an otherwise quiescent suspension and reported that interacting fibers settling in a dilute regime, $N < 1$, can settle faster than isolated fibers due to alignment with gravity and a tendency to form clumps or packets. This phenomenon may explain the strong settling observed by us at lower flow rates and low N. As the flow rate is increased, these effects would be diminished, since under shear flow, fiber orientations are more likely to be aligned with the flow direction and hydrodynamic stresses will tend to disrupt aggregates.

These results were obtained using one pipe diameter and pure cellulosic fibers. Other factors which are of practical interest and deserve future research include the influence of the ratio between pipe diameter and fiber dimensions, and the effects of changes in fibers hydrodynamic properties that may occur due to pretreatments or hydrolysis. In particular, changes in fiber flexibility and inter-fiber friction are variables known to influence the tendency of fibers to form strong networks.

4 Conclusions

The velocity profiles of cellulosic suspensions flowing in a horizontal pipe were measured using magnetic resonance flow imaging. The measured profiles depend strongly on fiber concentration, flow rate, and fiber type. The profile shapes varied greatly. We used measures of asymmetry and flatness as quantitative descriptors of the profile shape. We observed that (a) velocity profiles and pressure drops are similar to those of water at the lowest fiber concentrations; (b) velocity profiles with vertical asymmetry due to gravitational effects were found at fiber concentrations near $N = 3$. The asymmetry was more pronounced at lower flow rates; (c) symmetric and flat (plug flow) velocity profiles occur at high crowding numbers independent of the flow rate.

Our results show the existence of well-defined regions of high asymmetry in the concentration–flow rate plane. In such regions, the suspension does not satisfy the homogeneity requirement needed to use simple generalized Newtonian rheological models. Large changes in velocity asymmetry, flatness, and pressure drop occur as the concentration surpasses a critical value. The mass concentration at which this transition occurs is very different for fibers of different length. When stated in terms of crowding numbers, the transitions occurred at values of $N \approx 3$ for all fibers studied. The crowding number serves, therefore, as a useful indicator of the rheological state of a fiber suspension, especially in processes where fibers may change length, such as enzymatic hydrolysis. The maps presented in this work summarize the behavior of fiber suspensions in a wide range of conditions and are useful to identify regions where significant settling or excessive pressure drops are expected.

Acknowledgments Fiber length measurements were provided by Tom Lindström from Innventia AB, Stockholm, Sweden. Aspect Imaging, Hevel Modi'in Industrial Area, Shoham, Israel, provided pulse sequences used in the study. Partial financial support was provided by the Center for Process Analysis and Control, University of Washington, Seattle, WA. We acknowledge COST Action FP1005, which encouraged scientific interactions that helped in the interpretation of these data.

References

1. Kerekes, R.J.: Rheology of fibre suspensions in papermaking: an overview of recent research. Nordic Pulp Paper Res. J. **21**(5), 598–612 (2006)
2. Pimenova, N.V., Hanley, T.R.: Measurement of rheological properties of corn stover suspensions. Appl. Biochem. Biotechol **105–108**, 383–392 (2003)

3. Viamajala, S., McMillan, J.D., Schell, D.J., Elander, R.T.: Rheology of corn stover slurries at high solids concentrations—effects of saccharification and particle size. Bioresour. Technol. **100**, 925–934 (2009)
4. Knutsen, J.S., Liberatore, M.W.: Rheology of high-solids biomass slurries for biorefinery applications. J. Rheol. **53**(4), 877–892 (2009)
5. Stickel, J.J., Knutsen, J.S., Liberatore, M.W., Luu, W., Bousfield, D.W., Klingenberg, D.J., Scott, C.T., Root, T.W., Ehrhardt, M.R., Monz, T.O.: Rheology measurements of a biomass slurry: an inter-laboratory study. Rheol. Acta **48**, 1005–1015 (2009)
6. Duffy, G.G.: The significance of mechanistic-based models in fibre suspension flow. Nordic Pulp Paper Res. J. **18**(1), 74–80 (2003)
7. Hubbe, M.A.: Flocculation of cellulose fibers. Bioresources **2**(2), 296–331 (2007)
8. Mooney, C.A., Mansfield, S.D., Beatson, R.P., Saddler, J.N.: The effect of fiber characteristics on hydrolysis and cellulase accessibility to softwood substrates. Enzyme Microb. Technol. **25**(8–9), 644–650 (1999)
9. Lavenson, D.M., Tozzi, E.J., McCarthy, M.J., Powell, R.L.: Yield stress of pretreated corn stover suspensions using magnetic resonance imaging. Biotechnol. Bioeng. **108**, 2312–2319 (2011)
10. Altobelli, S.A., Givler, R.C., Fukushima, E.: Velocity and concentration measurements of suspensions by nuclear magnetic resonance imaging. J. Rheol. **35**(5), 721–734 (1991)
11. Ramachandran, A., Leighton, D.T.: Viscous resuspension in a tube: the impact of secondary flows resulting from second normal stress differences. Phys. Fluids **19**(5), 053301 (2007)
12. Kerekes, R.J., Schell, C.J.: Characterization of fibre flocculation regimes by a crowding factor. J. Pulp Paper Sci. **18**, 32–38 (1992)
13. Pulkkinen, I., Ala-Kaila, K., Aittamaa, J.: Characterization of wood fibers using fiber property distributions. Chem. Eng. Process **45**, 546–554 (2006)
14. Roche, C.M., Dibble, C.J., Knutsen, J.S., Stickel, J.J., Libratore, M.W.: Particle concentration and yield stress of biomass slurries during enzymatic hydrolysis at high-soids loadings. Biotechnol. Bioeng. (2009). doi:10.1002/bit.22381
15. Yan, Y., Koplik, J.: Transport and sedimentation of suspended particles in inertial pressure-driven flow. Phys. Fluids **21**(1), 1–9 (2009). doi:10.1063/1.3070919
16. Goudar, C.T., Sonnad, J.R.: Comparison of the iterative approximations of the Colebrook–White equation. Hydrocarbon Process. 79–84 (2008)
17. Herzhaft, B., Guazelli, E.: Experimental study of the sedimentation of dilute and semi-dilute suspensions of fibers. J. Fluid Mech. **384**, 133–158 (1999)